Engineering nanostructures with enhanced thermoplasmonic properties for biosensing and selective targeting applications

M. Essone Mezeme and C. Brosseau*

Université Européenne de Bretagne, Université de Brest, Lab-STICC, CS 93837, 6 avenue Le Gorgeu, 29238 Brest Cedex 3, France

(Received 17 September 2012; revised manuscript received 4 November 2012; published 28 January 2013)

This paper connects the study of thermoplasmonic properties in nanoscale particles with areas of biophysics involving a cell membrane with or without conductive pores. Using a quasistatic finite element modeling of the heat transfer equation in three dimensions we simulate the stationary heat generation and temperature field around several types of gold-based nanostructures. Models were constructed that emphasized the importance of obtaining precise temperature fields that might subsequently be used for biosensing and selective targeting applications. By analyzing the observed temperature increase, effective complex permittivity, and electric field enhancement that result from plasmonic resonance, this theoretical framework provides insight into the role of the nanoparticle shape in heat generation. To illustrate the usefulness of this approach for biosensing applications, we consider how the positioning of the nanoantenna affects heating efficiency. Linear response calculations of the temperature increase reveal that symmetric gold nanosphere dimers are not only suitable for sensing applications, but can also play the role of heat sources which are more efficient than the case of a single nanosphere. We also predict that this specific type of nanoantenna allows us to detect the presence and size of a hole in the cell membrane. These results provide insight into the physics of the cell membrane and provide guidance for more detailed studies of the nanoscale control of temperature in biological materials.

DOI: 10.1103/PhysRevE.87.012722 PACS number(s): 87.50.C−, 87.50.W−, 73.20.Mf

I. INTRODUCTION

Over the past few years, many studies of the effect of geometrical sensitivity of plasmon resonances of metallic and metallodielectric nanoparticles have shown that these artificial media structured on the subwavelength scale offer a wide range of photonic functionalities [1–10]. Some of the most interesting work in this field has focused on characterizing the scattering and absorption of electromagnetic radiation by nanometer-scale objects in the visible and infrared parts of the energy spectrum, not least in the hope of obtaining a better understanding of the large electromagnetic field enhancements on the nanoparticle surfaces [11–13]. High local-field enhancement in the vicinity of well-defined metal nanostructures when excited at their plasmon resonance can be created in a controlled manner by adjusting the physical parameters characterizing this system and the polarization of the external harmonic excitations [10,14,15].

In recent years thermoplasmonic properties of nanostructures have drawn significant interest both from a theoretical and experimental standpoint due to a myriad of potentially useful applications, e.g., light-harvesting devices [16,17]. A lesser-known application appears in the context of biology such as (selective) optical heating for photothermal therapy of cancers since gold nanostructures have their optical resonances associated with their surface plasmons within the transparency window of tissues (750–1100 nm), i.e., minimal absorption of water and hemoglobin, [12,13,18] and bacterial infections [19], easily conjugated to antibodies or proteins [12,20,21], minimal damage for the surrounding healthy tissues [21]. Plasmonic nano-objects owe their electromagnetic characteristics as much to their geometry (size, shape, and interparticle distance) as from the material from which they are composed [10,14,15,22]. There are a limited number of studies dealing with plasmonic nanoparticle arrays. One class of such arrays is exemplified by the measurements of the light concentration and heat generation in self-assembled plasmonic arrays composed of chains of 12 nm diam crystalline gold nanoparticles [23]. Planar clusters of coupled plasmonic nanoparticles, which support localized electric field enhancements and coherent effects, e.g., Fano resonances, have been also considered for their potential use in sensing applications [24]. Many varied numerical theoretical efforts have been made to understand the thermo-optical response of plasmonic nanostructures (see, e.g., Ref. [22]). Discrete dipole approximation and Mie scattering modeling for particles with arbitrary shapes have been quite popular [1,25,26]. For example, Florous and co-workers [1] have studied how thermo-optically plasmonic resonances of a variety of metal and metallodielectric nanostructures can be tuned by varying the temperature. Lereu and co-workers [27] investigated the thermal processes involved in thin plasmonic films and showed how to obtain the complex index of refraction of the thin metal films as a function of temperature and wavelength. Baffou and co-workers [28] argued that the plasmon-assisted photothermal response of nanoparticle-based systems can be evaluated by the boundary element method. They found that for a 100 nm gold sphere placed in water and illuminated by an incident light irradiance of 1 GW/m^2, the absorption power is $\approx$1 μW and the temperature increase of the nanoparticle is $\approx$50 K. These results were, in a sense, contrasting with the numerical estimates of several hundred degrees found in Ref. [29], or the 2200 K found in Refs. [21,30] for a single laser pulse. In addition, Baffou *et al.* observed a highly nonuniform temperature distribution at the nanoscale for assemblies of nanoparticles. Several authors [31–33] have studied the transient state of the temperature distribution before reaching the steady state in order to characterize the thermal storage properties of the embedding medium, e.g., water. They

*brosseau@univ-brest.fr

found that pulsed illumination does not necessarily achieve a much larger increase of temperature in the surrounding of the plasmonic nanostructure. Other authors [34] have also discussed the effect of plasmonic heat sources on the fluid flow, i.e., thermophoresis. Huang *et al.* [18] have also recently proposed a mathematical model for heating, heat transfer, and cellular injury and/or death for a laser-induced heating of gold nanorods. Based on this experimentally validated model, these authors were able to predict how selective binding of gold nanorods to cancer cells can influence the efficacy of extracellular hyperthermia. Since these studies, additional information has come forth about the design of optimized nanoheaters. Using the Green's function approach, Baffou *et al.* [31] studied the heat generation in gold nanostructures when illuminated at their plasmonic resonance. They found that elongated or sharp nanoparticles lead to much more efficient heaters than spherical nanoparticles. Interestingly, Baffou *et al.* [31] suggested that the steady-state temperature increase inside a homogeneous nanoparticle can be calculated from $\sigma_{\text{abs}}(\omega) I/4\pi\kappa r_e$, where $\sigma_{\text{abs}}(\omega)$ is the absorption scattering cross section, I is the irradiance of the exciting light, κ is the thermal conductivity of the nanoparticle, and r_e is a shape-dependent effective radius of the nanoparticle. Using a surface integral equation, Rodriguez-Oliveros and Sánchez-Gil reported similar results for gold nanostars (i.e., a nanoparticle with a starlike shape of various symmetries and tip numbers [35]). These authors found that a factor of 30 increase in the steady-state temperature can be obtained compared to that of the equivalent gold nanosphere having the same volume and the scattering to absorption cross section ratios can be tuned by varying the number and tip sharpness [35].

However, little focus has been paid to the interaction of thermoplasmonic nanostructures with biological cells and tissues. Two notable exceptions are Refs. [36,37]. In their study of photothermal destruction of murine macrophage cells by nanorods, Pissuwan and co-workers [36] pointed out that the effective temperature increase on the cells at a laser fluence of 30 J/cm^2 is of the order of 10 K. Interestingly, their finding suggests that heat stress instead of local melting of its membrane is the main cause of cell death. A theoretical investigation of the main effects during the interaction of a laser pulse with gold nanoparticles embedded in a liquid environment was also pioneered by Pustovalov and co-workers [21]. Pustovalov *et al.* argued that there could be several phenomena arising around the nanoparticle, i.e., thermal denaturation of proteins (323–433 K, depending on the laser time exposure), explosive evaporation of liquid accompanied by bubble formation and acoustic wave generation (373–1300 K), melting (1300–3000 K), explosion, and fragmentation. Another study by Tong *et al.* [37] of the photothermolysis mechanism showed that the laser energy used to destroy the cells when the nanoparticles are located on the cytoplasm membrane is one order of magnitude lower than that required when the nanoparticles are inside the cytoplasm. These authors have also suggested that the cell death is initiated by the disruption of the plasma membrane. A subsequent influx of Ca ions induces membrane blebbing and damage of the actin filaments, leading eventually to apoptosis. The importance of understanding how infrared light is absorbed by the cytoplasm lies primarily in determining the produced local heating and its effect on the physicochemical properties of the cell's membrane.

Theoretical studies of the dielectric properties of biological cells and tissues also have a long history, as reviewed in, e.g., Refs. [38–41]. In most of this body of works, a quasistatic field has been applied to the standard core-shell (CS) representation of a biological cell which has been the foundation on which our understanding of the dielectric properties of cells has been built [41]. While real cells have a highly heterogeneous structure, containing many constituents, i.e., salts, proteins, nucleic acids, reliable theoretical studies are difficult to implement for the complex models needed for these materials without making simplifying assumptions. Hence, we have not represented such details in our simulations which would enable a full comparison of the theoretical predictions with experimental data. A cell can be considered as a shelled particle with the inner medium exhibiting the same dielectric properties of the extracellular medium [38,39]. The surface of the cell is negatively charged for nearly all cells because of the predominance there of negatively charged groups, e.g., carboxylates, phosphates. This results in positive ions being attracted from the extracellular medium to the surface to form double layers [42]. The cytoplasm can be approximated as a highly conducting salt solution with a large concentration of dissolved organic material. From a physicochemical point of view, the cell membrane constitutes a region of low polarizability that can act as either a barrier to the passage of ions between two aqueous solutions, or, more likely, can act to slow down diffusion near cell boundaries by trapping diffusing particles. The membrane surrounding the cell has a lipid bilayer structure. It is very thin, typically 4–10 nm in thickness, and has incorporated into it large amounts of proteins. The induced potential drop, caused by low membrane permittivity and conductivity, as well as the rearrangement of interfacial charges, gives rise to field changes on the order of 1 kV cm^{-1} across the membrane thickness, for a 1 V cm^{-1} field strength. Here, we will assume electrically passive membranes, with no ion channels, ion pumps, or any change in the membrane conductance. Progress has been made in calculating and measuring the induced transmembrane voltage which is controlled by the shape membrane and charges at the cell membrane, the polarization, and the frequency of the exogenous electric field. All of this work has contributed significantly to a rich conceptual framework in correlating the morphological changes in cell transformations, e.g., mitosis, endocytosis, apoptosis, with their dielectric response [41,43–45].

Along with its fundamental importance, understanding the interactions of biological cells with nano-objects has important implications for medical imaging and for the development of biosensors. Here, due to the separation of scales between the sizes of the cell and the nanoantenna, we follow the spirit but not the letter of these approaches, by introducing a different three-dimensional (3D) multiphysics approach [46]. Inspired by these examples, we have looked anew at the heat generation by gold-based nanoparticles and its impact on nanoscale control of temperature for a cellular medium. The present study aims to contribute to an understanding of the plasmonic properties of nanoantennas inside or in the vicinity of a biological cell. A localized excitation, close to

the cell's membrane, could be used to probe for properties such as the surface charge distribution, topological defects, and mechanical stress. Here, we explore this question by using a numerical simulation of the heating efficiency of several kinds of nanostructures. The contributions of this study are twofold. First, we report on a set of calculations of the steady-state temperature field of gold-based nanoantennas. The paper quantifies the temperature increase broadenings and shifts with wavelength of the electromagnetic excitation and concludes that the anisotropy and symmetry of the nanoantenna are important factors to consider in selecting the type of nanoantenna used for heat efficiency. Temperature was obtained by considering the electromagnetic to heat conversion as a source term in the diffusive heat equation and solving Maxwell's equations by finite element simulations. Second, our results show that the temperature field is sensitive to variations in membrane characteristics, e.g., a hole in the membrane. We analyze this issue by using numerical examples with conductive pores in the membrane since it is well established that they lead to the interruption and saturation of the membrane charging process [47].

The paper is laid out in the following manner. In Sec. II we detail the method and the computational framework. The main results are presented in Sec. III. To illustrate the usefulness of this approach for biosensing applications, we consider several aspects of this study. First, we explore the geometric factors of the nanoantenna that control the temperature field. Second, we go on to discuss the influence of a hole in the cell's membrane on the temperature field. We also discuss some of the wider implications of these results. Section IV provides a final set of summary conclusions, and gives an outlook.

II. THEORETICAL MODEL AND COMPUTATIONAL DETAILS

To launch our topic, the particular implementation of the multiphysics approach is described as follows. For particles whose size R is much smaller than the wavelength λ of incident continuous-wave external illumination of the particle, the optical properties can be described within the quasistatic (dipole) approximation. Classical radiation theory [48] predicts that the ratio of the absorption to scattering cross sections varies as $(\lambda/R)^3$ for an incident monochromatic light interacting with a metal particle. Here the nanoparticle will be treated as a perfect absorber. That is, it is considered as an efficient converter of light to oscillatory energy of the electron plasma. Hence, scattering is not considered here.

The generic prescription for computing the temperature increase ΔT of the nanoantenna is different from that used by Baffou *et al.* [31], which is based on the boundary element method. At the large wavelength limit, the formulation simplifies to a set of two linear coupled partial differential equations for the potential and temperature profiles in the medium. By dint of the model developed in Refs. [14,15,48], we calculate the local electric field by solving self-consistently Laplace's equation, incorporating a position-dependent permittivity $\varepsilon(r) = \varepsilon'(r) - j\varepsilon''(r)$. This approach allows us to determine the electrostatic resonance, i.e., light absorption resonant with the nanoantenna plasmon energy. A more complete discussion of the derivation of the effective permittivity is given in Refs. [14,15]. Our model is completed by the standard conductive heat transfer equation (steady state) with the source supplied by light absorption [49], $\nabla \cdot [K(r)\nabla T(r)] = -h = -\omega\varepsilon''(r)\varepsilon_0 |E(r)|^2/2$, where $K(r)$ is the local thermal conductivity, $T(r)$ denotes the temperature distribution, ω is the angular frequency of the light, and $\varepsilon_0 \approx 8.85 \times 10^{-12}$ A^2 s^4 kg^{-1} m^{-3}. This equation describes the thermal dissipation of the light energy, i.e., Joule dissipation produced by the free electrons inside the particle [50]. The large length scales of the nanostructures (100–200 nm) and the small electron mean free path (in bulk Au $\approx$ 38 nm) suggest that electrons behave classically and transport is predominantly classical (Drude's model). We have verified that a finite-size correction has little effect on the analysis, and thus will be inconsequential for this range of frequencies [51].

We have solved our numerical problem by considering the following set of conditions: (i) The reference temperature is $T_0 = 37\,^\circ$C (body temperature); and (ii) the continuity of the normal component of heat flux at the boundaries, adiabatic boundaries of the computational domain, and the calculations use homogeneous Dirichlet-Neumann boundary conditions (see Refs. [14,15]) for the electrical potential. We have checked that our results are not sensitive to the particular value of the size L of the computational domain, as long as it satisfies the requirement that the nanoantenna sizes are sufficiently small compared to the wavelength of the incident wave (infinite wavelength framework) [52,53]. The calculations in this work were performed using the finite element method as implemented in the COMSOL MULTIPHYSICS code [54]. To reduce the cost of the computations, we used a cube computational domain and the nanoantenna was positioned at its center. Here $L = 1000$ nm. Table I lists the properties of the various phases considered in this study. For these parameter values, our model with a single gold nanosphere predicts that the effective complex permittivity is in quantitative agreement (not shown) with the Maxwell-Garnett mixing law, as expected due to the small volume fraction of the nanoantenna [52,55]. Before studying a complex system, it is instructive to consider a simple system for which ΔT can be solved exactly in the stationary state. Our numerical test addresses the situation considered by Govorov and co-workers [50], that is, a single gold spherical nanoparticle in water. Results for ΔT with respect to T_0 can be visualized when plotted as a function of the incident light irradiance $I = cn\varepsilon_0 |E|^2/2$ for different values of R, or as function of R for different values of I, where c is the speed of light in vacuum, and n is the refraction index of the external medium. The calculated ΔT agrees with previous analytical work showing that $\Delta T \propto \omega\varepsilon''(\omega) R^2 I$ [50]. An R^2 dependence is typical of the surface exchange of heat. As illustrated in Fig. 1, a good fitting to the data is obtained. Our results are also consistent with Baffou *et al.*'s observation that the heat generation can be strongly nonuniform [28]. These results compare also fairly well with similar calculations of Rodriguez-Oliveros and Sánchez-Gil [35].

The cell geometry that we consider in the following examples is composed of a perfectly flat insulating membrane of thickness $e = 5$ nm and a refractive index of 1.47. As mentioned earlier, the membrane thickness is so thin compared to the cell size that one can consider the membrane as flat.

TABLE I. Summary of the physical parameters used in our simulations.

	Gold nanoantenna	Cellular membrane	Intracellular medium	Extracellular medium
Index of refraction	Johnson-Christy [59]	1.47 [38–40]	1.36 [38–40]	1.33 [38–40]
Thermal conductivity [57] (W/m^3)	318	0.209	0.6	0.6

Performing such calculations would be very expensive in computational time and resources. In the following, the surrounding biological (extracellular and intracellular) medium will be described by an incompressible fluid (water) of negligible inertia and negligible absorption of radiation in the near-IR spectral range [26,48,50]. We shall assume that the nanoantenna is perfectly embedded in the intracellular (or extracellular) medium. Imperfect wetting and molecular coating at the gold-water interface are known to perturb the heat release [56]. The average computational time of a typical simulation for calculating ΔT corresponding to a configuration without cell is about 15 min, while 12 h are needed when a cell is present in the computational domain.

III. SIMULATIONS AND DISCUSSION

A. Quantifying the nanoantenna shape effect on the temperature increase

We are first interested in understanding how alternatives to the heavily studied spherical nanoantenna affect the wavelength shift and broadening of the ΔT spectrum. In this section, we investigate such nanostructures with gold volume held constant to 6×10^{-22} m^3. The simulations are performed with a typical 1 GW/m^2 of incident light irradiance. Results are shown in Fig. 2 for different shapes of the single particle and dimers, either symmetric or asymmetric, with a fixed gap distance d between particle surfaces. These spectral functions have other interesting features. Overall, one can conclude from those results that the shape anisotropy of the nanoantenna can significantly impact the temperature field along with

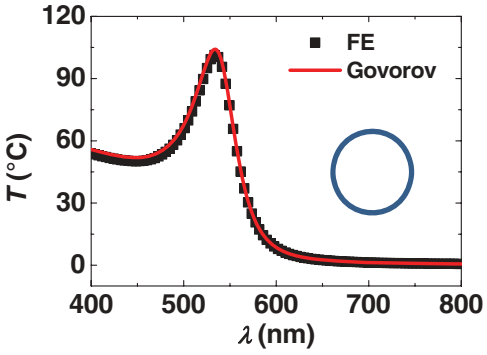

FIG. 1. (Color online) The temperature increase at the surface of a spherical gold nanoparticle in water as a function of wavelength of the incident light. The radius of the particle is set to $R = 50$ nm and the incident light irradiance is fixed at $I = 10^9$ W/m^2. The solid line designates Govorov's results [50] while square symbols designate our numerical data.

the electric characteristics. We have been able to find that among the four types of nanoantennas considered in Fig. 2, the symmetric dimer leads to a maximum temperature of 229 °C at 582 nm. The peak of the temperature increase is significantly redshifted and amplified by a factor of more than 2 by comparison to the case of a single sphere. We have confirmed that ΔT can be tuned by disymmetrizing the dimer [Fig. 2(d)]. Qualitatively similar results were obtained for sphere dimers [24,28,35,57,58] which can play the role of a much more efficient nanoheater than the sphere since they have larger absorption cross sections. It is also interesting to note that the larger ΔT [Fig. 2(d)] corresponds to the larger value of ε'' [Fig. 2(a)]. In addition, Fig. 2(b) shows that the anisotropic shape of the nanoantenna with an elongated tip has a large electric field enhancement (EFE) due to the tip plasmons, i.e., a factor of 10, but is associated with the smallest value of ΔT. In Fig. 2(d) we further compare the radius of an equivalent sphere R_{eq} obtained by using Govorov's dependence $\Delta T \propto R_{eq}^2$ [50] for the different shapes of the nanoantennas. It should be emphasized that the value R_{eq} for the symmetric dimer (75 nm) is larger than the radius of an equivalent nanosphere (65 nm) corresponding to the sum of two identical nanospheres of radius 46 nm. Thus, these calculations of the temperature increase reveal that symmetric gold nanosphere dimers are not only suitable for sensing applications, but can also play the role of heat sources which are more efficient than the case of a single nanosphere.

In addition, simulations were performed to investigate the influence of the gap distance d on the maximum temperature increase ΔT_{max} corresponding to the peak of $\Delta T(\lambda)$, ε''_{max} which is the maximum value of ε'', and wavelength λ_{max} corresponding to ε''_{max}. These simulations were conducted for symmetric and asymmetric dimers (Fig. 3). The temperature increase for the symmetric dimer is reduced by a factor of 4 when the gap distance is increased by a factor of 100. Disymmetrizing the dimer greatly decreases ΔT_{max} of the smallest nanosphere whereas the corresponding value for the largest nanosphere is weakly affected [Fig. 3(c)]. It is further shown that ε''_{max} [Fig. 3(b)] and λ_{max} [Fig. 3(a)] decrease as d is increased, although it is noticed that these parameters become constant upon a further increase of d above 100 nm. Such a result follows from the fact that, in the large gap distance ($d >$ diameter of the nanosphere $\approx$100 nm), the coupling of the surface plasmons of each individual nanostructure becomes weak. In contrast, for closely spaced nanospheres, the plasmonic response of two same-sized nanospheres shows a different coupling behavior than one sees in the heterodimer case. This is consistent with several recent works on the role played by symmetry breaking in nanoparticle systems on their plasmonic response [24].

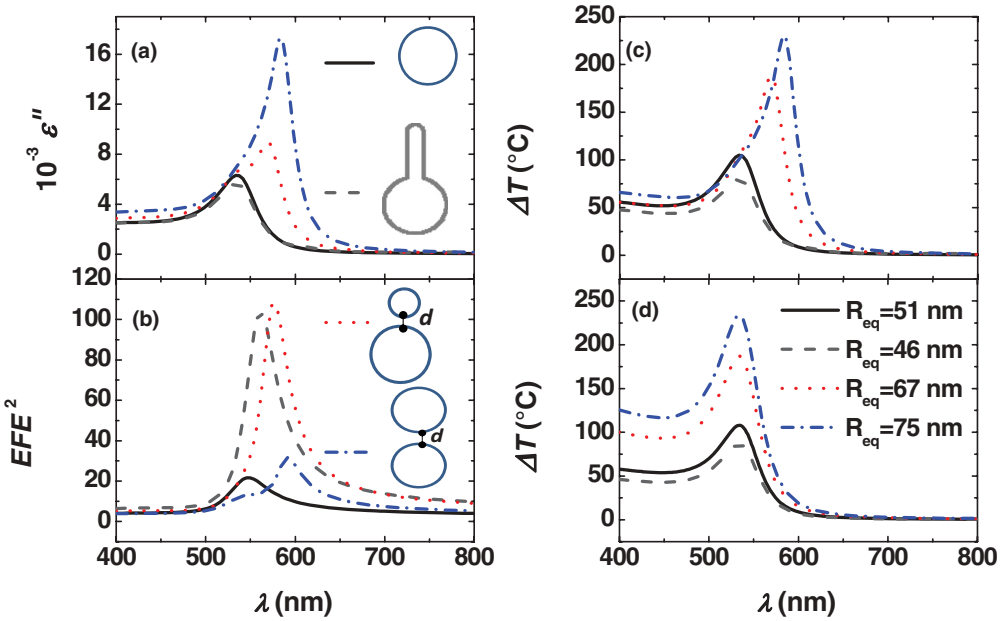

FIG. 2. (Color online) (a) shows the imaginary part of the effective permittivity for different types of gold nanoantennas immersed in water as a function of the wavelength of the incident light. In the inset, we see the nanoantenna shape. The electric field orientation is indicated by the arrow. In all systems, we considered a gold volume fraction set to 5.5×10^{-4}. The gap distance between particle surfaces is set to $d = 5$ nm. (b) shows the corresponding square of electric field enhancement (EFE). (c) shows the corresponding temperature increase. (d) shows the equivalent radius R_{eq} obtained by using Govorov's dependence $\Delta T \propto R_{eq}^2$ [50] for the different shapes of nanoantennas. In all results given here, the incident light irradiance is fixed at $I = 10^9$ W/m^2.

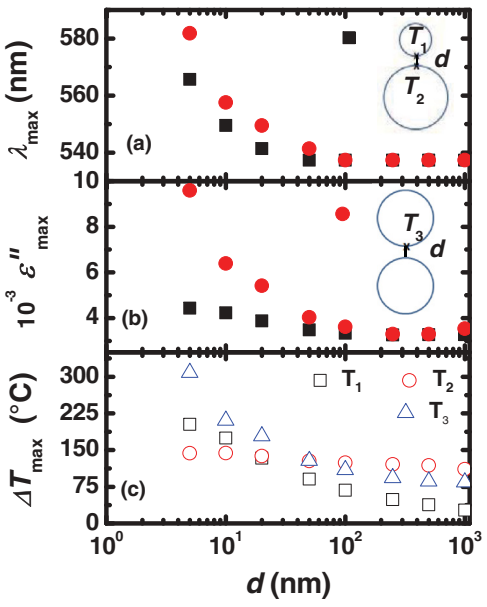

FIG. 3. (Color online) (a) shows the calculated wavelength corresponding to the maximum of ε'' as function of the gap distance d for the symmetric (two same-sized nanospheres of radius $R = 41$ nm) and asymmetric (the radii of the small and large spheres are, respectively, 22 and 50 nm) dimers shown in the inset. In both cases, the gold volume held constant to 6×10^{-22} m^3. (b) shows the corresponding maximum of ε''. (c) shows the corresponding maximum temperature increase. In all results given here, the incident light irradiance is fixed at $I = 10^9$ W/m^2. Symbols T_i indicate points at the surface of the nanoparticles such as described in the inset of (a) and (b).

B. Characterizing the positioning of the nanoantenna with respect to the membrane

We now turn to our main objective of investigating the coupling between the nanoantenna and the cell membrane. The simulations are performed with a typical 10^{-2} GW/m^2 of incident light irradiance. We reproduced the same simulations as above with different situations with the nanoantenna inside or outside the cellular medium, and with the two nanospheres on both sides of the membrane in the case of a symmetric dimer with the gap distance d between the two nanospheres set to 7 nm. In Figs. 4(a) and 4(b) we compare the permittivity frequency and ΔT profiles for three representative cases. Two interesting features are noticed. First, when the two nanospheres are either inside [case "in" displayed in Figs. 4(a) and 4(b)] or outside [case "ex" displayed in Figs. 4(a) and 4(b)] the cytoplasm, the plasmon resonance, and the extracted ΔT are only weakly affected. Second, the interesting case corresponds to the situation where the two nanospheres are on both sides of the membrane [case "ex-in" displayed in Figs. 4(a) and 4(b)] and in close proximity to it. Here, the peak of ΔT is significantly larger compared to the other cases. As a consequence, the primary conclusion from these data is that tracking the cell's membrane can be quantified by an adiabatic temperature change that occurs when an external field excites the plasmonic resonance of a nanosphere dimer configuration.

C. Perforating the membrane

Next, we use our model to quantitatively analyze the case of punctured membranes using the simplest model of the hole, described as a cylindrical opening in the flat membrane.

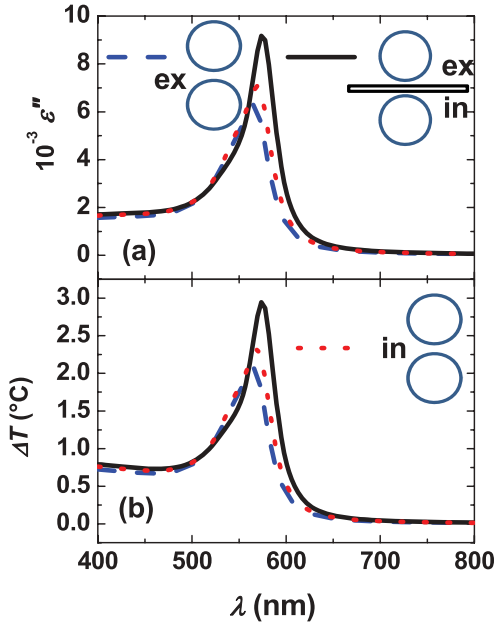

FIG. 4. (Color online) (a) The imaginary part of the effective permittivity as a function of the wavelength of the incident light for three situations considered: two nanospheres placed within the extracellular medium (ex), one nanosphere is placed in the extracellular medium while the other is in the intracellular medium (ex-in), and two nanospheres placed within the intracellular medium (in). In all results given here $R = 41$ nm, $d = 7$ nm, and the incident light irradiance is fixed at $I = 10^7$ W/m^2. (b) Same as in (a) for the temperature increase.

Figures 5(a) and 5(b) are a plot of ε'' and ΔT against the wavelength of the incident light for the symmetric gold sphere dimer and a membrane containing a hole of dimension l. A number of remarks are in order. First, a significant blueshift is evidenced as the hole size is increased. Second, the larger is the hole, the smaller are the peaks of ε'' and ΔT. Interestingly, in Fig. 6(a) we show the electric field enhancement (EFE), with a corresponding heat source density [Fig. 6(b)] and temperature increase [Fig. 6(c)] for a gold dimer placed in the vicinity of a cell membrane with a single hole of size $\ell = 100$ nm. The selected wavelength, 565 nm, of light exciting the gold nanosphere dimer corresponds to the peak of ΔT shown in Fig. 5. Altogether, these numerical calculations provide estimates of the maximum EFE ≈ 100 which is localized inside the hole, whereas the hot spots related to the maximum value of the heat source density $h \approx 4$ nW/nm^3 are localized respectively in the near vicinity of the south and north poles in the inner parts of the nanospheres.

To examine the impact of the hole size in the membrane on the thermal behavior, $\Delta T_{\max}$ is plotted for different ℓ in Fig. 7. The numerical hole size range of this study lies between typical values reported in the literature [60]; the exact experimental hole size range is dependent on the kind of cell. As ℓ increases, $\Delta T_{\max}$ decreases monotonically because more of the heat diffuses through the cell's membrane. This result is of both fundamental, e.g., molecular processes involved in membrane optoporation, and practical importance, e.g., transdermal drug delivery, transport of drugs, oligonucleotides, antibodies, and plasmids across cell membranes. Even though

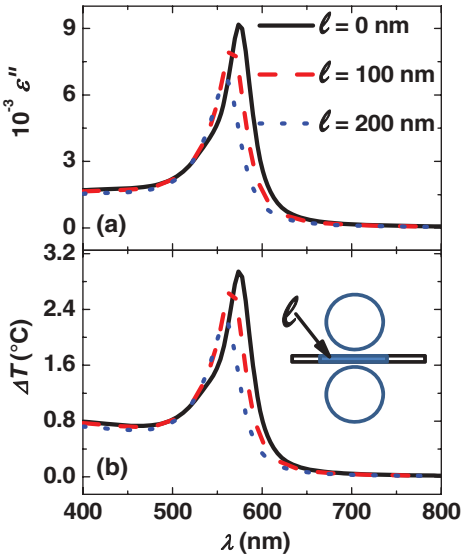

FIG. 5. (Color online) The imaginary part of the effective permittivity as a function of the wavelength of the incident light for a gold nanosphere dimer placed in the vicinity of a cell membrane containing a hole of size ℓ. In all results given here $R = 41$ nm, $d = 7$ nm, and the incident light irradiance is fixed at $I = 10^7$ W/m^2. (b) Same as in (a) for the temperature increase. The exciting electric field is oriented perpendicularly to the membrane's plane.

the exact mechanisms behind electroporation and optoporation are still debated, there exists some agreement that, for real biological cells, multiple and smaller transient (nucleated

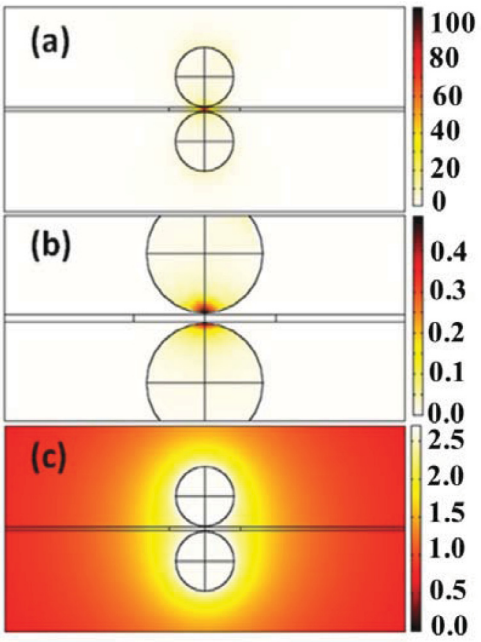

FIG. 6. (Color online) (a) Spatial distribution of the electric field enhancement for a gold nanosphere dimer placed in the vicinity of a cell membrane. The exciting electric field is oriented perpendicularly to the membrane's plane. $\ell = 100$ nm and $\lambda = 565$ nm. (b) Corresponding heat source density h (μW/nm^3). (c) Corresponding steady-state temperature increase ΔT (°C). In all results given here, the incident light irradiance is fixed at $I = 10^7$ W/m^2.

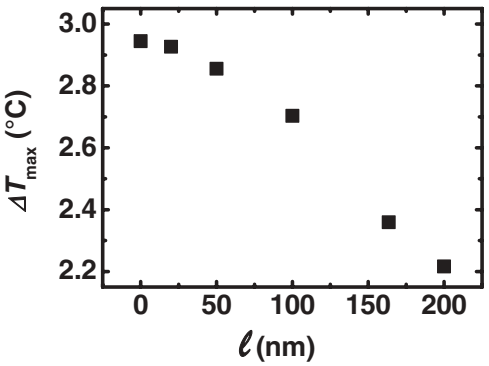

FIG. 7. Maximum temperature increase as a function of the hole size for a gold nanosphere (41 nm) dimer placed in the vicinity of a cell membrane. The exciting electric field is oriented perpendicularly to the membrane's plane. In all results given here, the incident light irradiance is fixed at $I = 10^7$ W/m^2.

independently) pores are closer to reality than the large pores in flat membranes we have considered in this model [61].

D. Discussion

Finally, we comment on the implications for selective targeting and biosensing applications of these label-free detection plasmonic nanoantennas. Prior studies of thermoplasmonic nanostructures have shown convincingly that they can act as controlled nanoheaters, i.e., photothermal therapy agents, and can be used to destruct malignant cells and tissues [62]. In addition, the toxicity and cellular impact of gold nanoparticles both *in vitro* and *in vivo* were discussed in many scientific reports (see, e.g., Ref. [63] and references therein). Our observation here represents a clear-cut case of an optimized plasmonic nanoantenna where a temperature increase at specific cell boundaries is predicted. When the exciting electric field is polarized along the axis connecting the two nanospheres of the dimer there is a strong surface plasmon coupling. Thus, the associated temperature increases in the vicinity of the dimer. However, if the excitation is not polarized along the dimer axis, we find a much weaker temperature increase (not shown). This means that the two nanospheres are decoupled, supporting the experimental observations of Yang and co-workers [64].

The presented technique has also a great potential for application in tissue engineering. To this end, we need to improve multicellular simulations [45]. The results presented above consider a flat, isotropic, and indeformable membrane placed perpendicularly to the electric field lines. Since the local stresses and strains in the cells and their surrounding environment can be directly numerically determinable, a more accurate calculation based on electromechanical Maxwell stresses [61,65] can solve these problems. A crucial feature common to biological membranes is the phospholipid bilayer. The expected discontinuous change of the order parameter at the sol-gel transition involves a large entropy content which is at the origin of the decrease of mobility in the gel phase. Recent observations by Urban and co-workers [66] provides direct evidence that how gold nanoparticles motion can reveal local information on the dynamics of the reversible sol-gel transition of phospholipid giant unilamellar vesicles as a model system for the biological cell membrane. In a related context, Bendix and co-workers [67] performed direct measurements of the temperature profile surrounding gold nanoparticles optically trapped on a lipid bilayer. Both nanoparticle size and optical irradiance control the particle temperature and heating on a subwavelength scale.

Previous experiments and models of membrane pore formation (see, e.g., Ref. [68]) suggested that gold nanoparticles can be used to selectively deliver molecules into cells. Thermal fluctuations can cause spontaneous pore formation but are rare due to their high free-energy barriers [69]. Even for model lipid bilayer membranes, there is a lack of experimental data to compare to when validating numerical simulations. Based on a coarse-grained amphiphilic model, Tolpekina and co-workers [70] found that the cost of pore formation is $\approx$15–20kT, where k is Boltzmann's constant. Since plasmon resonance is strongly dependent on the local environment of the membrane cell, the functional $\Delta T\,(\lambda)$ is particularly suited for sensing applications of a large variety of cellular processes ranging from intracellular trafficking, morphological differentiation, and fusion. Urban and co-workers [71] have reported a detailed study of an all-optical contactless injection of gold nanoparticles through phospholipid membranes. The combination of simultaneous optical heating of a gold nanoparticle exposed to laser light tuned to the plasmon resonance of the nanoparticle and strong optical forces acting on the nanoparticle to push it into the vesicle provides a rare opportunity to study the actual physical mechanisms underlying electroporation of cells, e.g., electromechanical instability, and the characteristic time scales involved in the pore opening. These experimental observations provide a simple model to quantitatively relate optoporation of a single cell (and assemblies of cells modeling a tissue) and the local change of their dielectric and thermal properties.

The essential physics of this system can be further elaborated in terms of a related multiphysics effect, i.e., the electrocaloric effect [72]. Prior studies [72] have shown that the general form of the temperature change under an adiabatic electric field variation from the initial value $E_\mathrm{i} = 0$ to final value $E_\mathrm{f} = E$ is $\Delta T = -\frac{T}{C_\mathrm{E}} \int_0^E (\frac{\partial P}{\partial T})_E dE$, where C_E is the volume specific heat at constant field, and P is the electric polarization originating from charge and electric multipole moments. Ignoring the temperature dependence of C_E and assuming that the entropy change $\Delta S = S(P) - S(P = 0)$ is proportional to P^2, one finds that $\Delta T \propto \frac{T}{C_\mathrm{E}} P^2$ [69]. In our case, the polarization is tuned with the external field. This analysis reveals a strong sensitivity of ΔT to the local electric field. At the same time, the Govorov mode predicts a maximum of ΔT corresponding to the maximum of ε'' [50]. These predictions match qualitatively our numerical observations.

IV. SUMMARY AND PERSPECTIVES

We may now summarize our results: We have combined quasistatic calculations of the effective permittivity and thermostatic calculations of the temperature increase in gold-based nanostructures in the infrared frequency range. The extensive numerical simulations presented here showed that strong electric field enhancement and heat generation confinement can be achieved even for simple geometries of

optical nanoantennas. In the particular case studied, that of a symmetric gold sphere dimer, the computations predict that it plays the role of a heating amplifier. We predict that this specific type of nanoantenna allows us to detect the presence and size of a hole in the cell membrane. As we have seen from our earlier simulations [14,15], a good diagnostic of the membrane poration can be obtained by observing the induced transmembrane voltage (ITV). Indeed, over the past decades ITV has become an established experimental technique for probing the electroporation of cells and tissues.

There are a number of ways in which the approach could be developed further. The route to more sophisticated simulations of thermoplasmonic properties of nanoantennas is clear. First, it would be of interest to study the nonstationary temperature field and measure the typical time scale required to reach the steady-state regime [26,32,33]. Second, we need to study the thermoplasmonic response of such nanoantennas when a surface density of free charges is present at the outer and inner surface of the membrane as compared with that predicted with no surface charge. Third, the above calculation is only valid in the limit of a flat membrane. Lipid membranes are very flexible, and under thermal perturbations they undergo surface deformations that are significantly larger than their thicknesses. These membrane deformations may mediate interactions between the membrane and nano-objects which are in its close proximity. The same calculations can be performed for a membrane with a corrugated surface. There is also clear interest in looking at specific multifunctional nanoparticles that combine targeting, therapeutic, and diagnostic functionalities [12]. Considering these directions for future study, it is our hope that the methods investigated here may establish themselves as an important tool for sensing and selective targeting applications of cellular media for which the control of temperature of a few degrees at the nanoscale is needed.

ACKNOWLEDGMENTS

We acknowledge the support of the Ph.D. funding programme (Grant Programme No. 211-B2-9/ARED) of the Conseil Régional de Bretagne and the Ph.D. mobility program of Université de Brest. The Lab-STICC is Unité Mixte de Recherche CNRS 6285.

[1] B. Khlebtsov, V. Zharov, A. Melnikov, V. Tuchin, and N. Khlebtsov, Nanotechnology **17**, 5167 (2006).

[2] V. Myroshnychenko, E. Carbó-Argibay, L. Pastoriza-Santos, J. Pérez-Juste, L. M. Liz-Marzán, and F. J. Garcia de Abajo, Adv. Mater. **20**, 4288 (2008); V. Myroshnychenko, J. Rodríguez-Fernández, L. Pastoriza-Santos, A. M. Funston, C. Novo, P. Mulvaney, L. M. Liz-Marzán, and F. J. García de Abajo, Chem. Soc. Rev. **37**, 1792 (2008).

[3] S. A. Meier, M. L. Brongersma, P. G. Kik, S. Meltzer, A. A. G. Requicha, and H. A. Atwater, Adv. Mater. **13**, 1501 (2001).

[4] W. L. Barnes, A. Dereux, and T. W. Ebbesen, Nature (London) **424**, 824 (2003).

[5] W. Cai and V. Shalaev, *Optical Metamaterials: Fundamentals and Applications* (Springer, New York, 2009).

[6] L. Novotny and B. Hecht, *Principles of Nano-Optics* (Cambridge University, Cambridge, UK, 2006).

[7] M. A. Barral and A. M. Llois, Science **297**, 1160 (2002).

[8] N. J. Halas, S. Lal, C. Wei-Shun, S. Link, and P. Nordlander, Chem. Rev. **111**, 3913 (2011).

[9] S. V. Boriskina and B. M. Reinhard, Nanoscale **4**, 76 (2012).

[10] M. I. Stockman, Phys. Today **64**, 39 (2011); Opt. Express **19**, 22029 (2011).

[11] A. Mejdoubi, M. Essone Mezeme, Z. Sekkat, M. Bousmina, and C. Brosseau, J. Appl. Phys. **110**, 103105 (2011).

[12] X. Huang, I. H. El-Sayed, W. Qian, and M. A. El-Sayed, J. Am. Chem. Soc. **128**, 2115 (2006); V. P. Zharov, E. N. Galitovskaya, C. Johnson, and T. Kelly, Laser Med Surg. **37**, 219 (2005); C. A. Loo, A. Lowery, N. Halas, J. West, and R. Drezek, Nano Lett. **5**, 705 (2005); W. Zhao and J. M. Karp, Nat. Mater. **8**, 453 (2009); I. H. El-Sayed, X. Huang, and M. A. El-Sayed, Cancer Lett. **239**, 129 (2006); G. S. Terentyuk, G. N. Maslyakova, L. V. Suleymanova, N. G. Khlebtsov, B. N. Khlebtsov, G. G. Akchurin, I. L. Maksimova, and V. V. Tuchin, J. Biomed. Opt. **14**, 021016 (2009); R. Bardhan, S. Lal, A. Joshi, and N. J. Halas, Acc. Chem. Res. **44**, 936 (2011); C. Hrelescu, T. K. Sau, A. L. Rogach, F. Jäckel, G. Laurent, L. Douillard, and F. Charra, Nano Lett. **11**, 402 (2011).

[13] L. C. Kennedy, L. R. Bickford, N. A. Lewinski, A. J. Coughlin, Y. Hu, E. S. Dray, J. L. West, and R. A. Drezek, Small **7**, 169 (2011).

[14] M. Essone Mezeme, S. Lasquellec, and C. Brosseau, Phys. Rev. E **84**, 026612 (2011).

[15] M. Essone Mezeme, S. Lasquellec, and C. Brosseau, Phys. Rev. E **81**, 057602 (2010).

[16] A. Aubry, D. Y. Lei, A. Fernàndez-Dominguez, Y. Sonnefraud, S. A. Maier, and J. B. Pendry, Nano Lett. **10**, 2574 (2010).

[17] E. Rousseau, A. Siria, G. Joudan, S. Volz, F. Comin, J. Chevrier, and J. J. Greffet, Nat. Photon. **3**, 514 (2009); G. Dominguez, S. Volz, K. Joulain, and J. J. Greffet, Phys. Rev. Lett. **94**, 085901 (2005); Y. de Wilde, F. Formanek, R. Carminati, B. Gralak, P. A. Lemoine, K. Joulain, J. P. Mulet, Y. Chen, and J. J. Greffet, Nature (London) **444**, 740 (2006).

[18] H.-C. Huang, K. Rege, and J. J. Heys, ACS Nano **4**, 2892 (2010).

[19] J. R. Lakowicz, Plasmonics **1**, 5 (2006).

[20] V. P. Zharov, R. R. Letfullin, and E. N. Galitovskaya, J. Phys. D **38**, 2571 (2005); R. R. Letfullin, C. Joenathan, T. F. George, and V. P. Zharov, Nanomedicine **1**, 473 (2006).

[21] V. K. Pustovalov and V. A. Babenko, Laser Phys. Lett. **1**, 516 (2004); **2**, 84 (2005).

[22] I. Tsukerman, *Computational Methods for Nanoscale Applications: Particles, Plasmons, and Waves* (Springer, New York, 2007).

[23] A. Sanchot, G. Baffou, R. Marty, A. Arbouet, R. Quidant, C. Girard, and E. Dujardin, ACS Nano **6**, 3434 (2012).

[24] F. Wen, J. Ye, N. Liu, P. Van Dorpe, P. Nordlander, and N. J. Halas, Nano Lett. **12**, 5020 (2012); N. J. Halas, S. Lal, S. Link, W.- S. Chang, D. Natelson, J. H. Hafner, and P. Nordlander, Adv. Mater. **24**, 4842 (2012).

[25] N. J. Florous, K. Saitoh, and M. Koshiba, IEEE Trans. Nanotechnol. **6**, 549 (2007).

[26] N. G. Khlebtsov, Quantum Electron. **38**, 504 (2008).

[27] A. L. Lereu, A. Passian, R. H. Farahi, N. F. Van Hulst, T. L. Ferrell, and T. Thundat, J. Vac. Sci. Technol. A **26**, 836 (2008).

[28] G. Baffou, R. Quidant, and F. J. García de Abajo, ACS Nano **4**, 709 (2010).

[29] P. M. Bendix, S. N. S. Reihani, and L. B. Oddershede, ACS Nano **4**, 2256 (2010).

[30] C. M. Pitsillides, E. K. Joe, X. Wei, R. R. Anderson, and C. P. Lin, Biophys. J. **84**, 4023 (2003).

[31] G. Baffou, R. Quidant, and C. Girard, Appl. Phys. Lett. **94**, 153109 (2009); Phys. Rev. B **82**, 165424 (2010).

[32] Y. A. Avetisyan, A. N. Yakunin, and V. V. Tuchin, Appl. Opt. **51**, C88 (2012).

[33] E. Sassaroli, K. C. P. Li, and B. E. O'Neill, Phys. Med. Biol. **54**, 5541 (2009).

[34] S. Duhr and D. Braun, Proc. Natl. Acad. Sci. USA **103**, 19678 (2006); T. Kang, S. Hong, Y. Choi, and L. P. Lee, Small **6**, 2649 (2010).

[35] R. Rodriguez-Oliveros and J. A. Sánchez-Gil, Opt. Express **20**, 621 (2012).

[36] D. Pissuwan, S. M. Valenzuela, M. C. Killingsworth, X. Xu, and M. B. Cortie, J. Nanopart. Res. **9**, 1109 (2007).

[37] L. Tong, Y. Zhao, T. B. Huff, M. N. Hansen, A. Wei, and J. X. Cheng, Adv. Mater. **19**, 3136 (2007).

[38] R. Pethig, *Dielectric and Electronic Properties of Biological Materials* (Wiley, New York, 1979); K. R. Foster and H. P. Schwan, Crit. Rev. Biomed. Eng. **17**, 25 (1989).

[39] K. Asami, T. Hanai, and N. Koizumi, Jpn. J. Appl. Phys. **19**, 359 (1980); K. Asami, Prog. Polym. Sci. **27**, 1617 (2002); J. Phys. D **39**, 492 (2006); **41**, 085501 (2008).

[40] P. Salou, A. Mejdoubi, and C. Brosseau, J. Appl. Phys. **105**, 114702 (2009); C. Fourn, S. Lasquellec, and C. Brosseau, *ibid.* **102**, 124107 (2007); C. Fourn and C. Brosseau, Phys. Rev. E **77**, 016603 (2008); M. Essone Mezeme, S. Lasquellec, and C. Brosseau, J. Phys. D **42**, 135420 (2009); M. Essone Mezeme and C. Brosseau, J. Appl. Phys. **107**, 014701 (2010); **108**, 014701 (2010); M. Essone Mezeme, S. Lasquellec, and C. Brosseau, *ibid.* **109**, 014302 (2011).

[41] H. P. Schwan, Adv. Biol. Med. Phys. **5**, 147 (1957); H. P. Schwan, in *Interactions Between Electromagnetic Fields and Cells*, edited by A. Chiabrera, C. Nicolini, and H. P. Schwan (Plenum, New York, 1985), pp. 1–18; K. R. Foster and H. P. Schwan, Crit. Rev. Biomed. Eng. **17**, 25 (1989); H. Pauly and H. P. Schwan, Z. Naturforsch. B **14**, 125 (1959); K. R. Foster and H. P. Schwan, in *Handbook of Biological Effects of Electromagnetic Fields*, edited by C. Polk and E. Postow (CRC, New York, 1996), pp. 25–102; H. P. Schwan, IEEE Trans. Electr. Insul. **20**, 913 (1985).

[42] G. Cevc, Biochim. Biophys. Acta **1031**, 311 (1999).

[43] J. C. Weaver and Y. A. Chizmadzhev, Bioelectrochem. Bioenerg. **41**, 135 (1996).

[44] M. Essone Mezeme, G. Pucihar, M. Pavlin, C. Brosseau, and D. Miklavčič, Appl. Phys. Lett. **100**, 143701 (2012).

[45] M. Essone Mezeme, M. Kranjc, F. Bajd, I. Serša, C. Brosseau, and D. Miklavčič, Appl. Phys. Lett. **101**, 213702 (2012).

[46] W. B. J. Zimmerman, *Multiphysics Modelling with Finite Element Methods* (World Scientific, London, 2006).

[47] R. Sauvé and S. Ohki, J. Theor. Biol. **81**, 157 (1979).

[48] C. F. Bohren and D. R. Huffman, *Absorption and Scattering of Light by Small Particles* (Wiley, New York, 1998).

[49] Z. M. Zhang, *Nano/Microscale Heat Transfer* (McGraw-Hill, New York, 2007); see also *Microscale and Nanoscale Heat Transfer*, edited by S. Volz (Springer, Berlin, 2007).

[50] A. O. Govorov, W. Zhang, T. Skeini, H. H. Richardson, J. Lee, and N. A. Kotov, Nanoscale Res. Lett. **1**, 84 (2006); H. H. Richardson, M. T. Carslon, P. J. Tandler, P. Hernandez, and A. O. Govorov, Nano Lett. **9**, 1139 (2009).

[51] J. Zuloaga, E. Prodan, and P. Nordlander, Nano Lett. **9**, 887 (2009); J. M. McMahon, S. K. Gray, and G. C. Schatz, *ibid.* **10**, 3473 (2010).

[52] S. Torquato, *Random Heterogeneous Materials: Microstructure and Macroscopic Properties* (Springer, New York, 2002).

[53] M. Sahimi, *Applications of Percolation Theory* (Taylor & Francis, London, 1994); *Heterogeneous Materials I: Linear Transport and Optical Properties* (Springer, New York, 2003); G. I. Barenblatt, *Scaling* (Cambridge University Press, New York, 2004).

[54] COMSOL MULTIPHYSICS version 3.4.

[55] C. Brosseau (unpublished).

[56] O. M. Wilson, X. Hu, D. G. Cahill, and P. V. Braun, Phys. Rev. B **66**, 224301 (2002); J. Alper and K. Hamad-Schifferli, Langmuir **26**, 3786 (2010).

[57] H. Wang, Y. Wu, B. Lassiter, C. L. Nehl, J. H. Hafner, P. Nordlander, and N. J. Halas, Proc. Natl. Acad. Sci. USA **103**, 10856 (2006).

[58] A. Christ, O. J. F. Martin, Y. Ekinci, N. A. Gippius, and S. G. Tikhodeev, Nano Lett. **8**, 2171 (2008).

[59] P. B. Johnson and R. W. Christy, Phys. Rev. B **6**, 4370 (1972).

[60] D. C. Chang and T. S. Reese, Biophys. J. **58**, 1 (1990); C. Wilhelm, M. Winterhalter, U. Zimmermann, and R. Benz, *ibid.* **64**, 121 (1993); P. Soman, W. Zhang, A. Umeda, Z. J. Zhang, and S. Chen, J. Biomed. Nanotechnol. **7**, 1 (2011); A. Hai and M. E. Spira, Lab. Chip **12**, 2865 (2012).

[61] H. Isambert, Phys. Rev. Lett. **80**, 3404 (1998); D. P. Tieleman, BMC Biochem. **5**, 10 (2004).

[62] I. H. El-Sayed, X. Huang, and M. A. El-Sayed, Nano Lett. **5**, 829 (2005); L. Hirsch, R. Stafford, J. Bankson, S. Sershen, B. Rivera, R. Price, J. Hazle, N. Halas, and J. West, Proc. Natl. Acad. Sci. USA **100**, 13549 (2003).

[63] A. M. Alkilany and C. J. Murphy, J. Nanopart. Res. **12**, 2313 (2010).

[64] L. Yang, H. Wang, B. Yan, and B. M. Reinhard, J. Phys. Chem. C **114**, 4901 (2010).

[65] G. Bryant and J. Wolfe, J. Membr. Biol. **96**, 129 (1987); I. V. Timoshkin, S. J. MacGregor, R. A. Fouracre, B. H. Crichton, and J. G. Anderson, J. Phys. D **39**, 596 (2006).

[66] A. S. Urban, M. Fedoruk, M. R. Horton, J. O. Rädler, F. D. Stefani, and J. Feldmann, Nano Lett. **9**, 2903 (2009).

[67] J. R. Hendriksen and T. L. Andresen, Biophys. J. **101**, 100 (2011).

[68] V. Oliynyk, U. Kaatze, and T. Heimburg, Biochim. Biophys. Acta **1768**, 236 (2007); R. A. Sperling, P. R. Gil, F. Zhang, M. Zanella, and W. J. Parak, Chem. Soc. Rev. **37**, 1896 (2008).

[69] D. Sornette and N. Ostrowsky, in *Micelles, Membranes, Micro-Emulsions and Monolayers*, edited by W. M. Gelbart, A. Ben-Shaul, and D. Roux (Springer, Berlin, 1994); P.-G. de Gennes, F. Brochard-Wyart, and D. Quéré, *Capillarity and Wetting Phenomena: Drops, Bubbles, Pearls, Waves* (Springer, New York, 2004).

[70] T. V. Tolpekina, W. K. den Otter, and W. J. Briels, J. Chem. Phys. **121**, 8014 (2004).

[71] A. S. Urban, T. Pfeiffer, M. Fedoruk, A. A. Lutich, and J. Feldmann, ACS Nano **5**, 3585 (2011).

[72] A. S. Mischenko, Q. Zhang, J. F. Scott, R. W. Whatmore, and N. D. Mathur, Science **311**, 1270 (2006); T. Castán, A. Planes, and A. Saxena, Phys. Rev. B **85**, 144429 (2012); see also A. M. Tishin and Y. I. Spichkin, *The Magnetocaloric Effect and Its Applications* (IOP, Bristol, UK, 2003).